Catalysis Today xxx (2015) xxx–xxx

Contents lists available at ScienceDirect

Catalysis Today

journal homepage: www.elsevier.com/locate/cattod

Ru nanoparticles confined in Zr-containing spherical mesoporous silica containers for hydrogenation of levulinic acid and its esters into γ-valerolactone at ambient conditions

Yasutaka Kuwahara[a,b], Yasuhiro Magatani[a], Hiromi Yamashita[a,b,*]

[a] Division of Materials and Manufacturing Science, Graduate School of Engineering, Osaka University, 2-1 Yamadaoka, Suita, Osaka 565-0871, Japan
[b] Unit of Elements Strategy Initiative for Catalysts & Batteries (ESICB), Kyoto University, Katsura, Kyoto 615-8520, Japan

ARTICLE INFO

Article history:
Received 10 November 2014
Received in revised form 12 January 2015
Accepted 14 January 2015
Available online xxx

Keywords:
Metal nanoparticles
Mesoporous silica
Hydrogenation
Biomass conversion
Levulinic acid
γ-Valerolactone

ABSTRACT

Hydrogenation of levulinic acid and its esters to produce γ-valerolactone (GVL) was demonstrated over ruthenium nanoparticle (NP) catalyst supported on Zr-containing spherical mesoporous silicas as a bifunctional catalyst. The Ru NPs were found to be uniformly dispersed within the periodically ordered short mesopore channels with an average size of less than 1.5 nm without any agglomeration. They exhibited superior activity for the hydrogenation of both levulinic acid and its esters under mild reaction conditions (70 °C, 0.5 MPa H_2) compared to those supported on the conventional silica owing to their ultrasmall particle size and the acidity of Zr sites. In the hydrogenation of levulinate ester, addition of heterogeneous acids could afford a faster reaction rate in GVL production by accelerating the following intramolecular dealcoholation step. The catalyst was reusable over repeated catalytic cycles without a significant loss of catalytic performance, demonstrating its potential as a heterogeneous catalyst for GVL production under ambient reaction conditions.

1. Introduction

Efficient and sustainable biomass conversion technologies are being extensively studied to address worldwide concerns about the depletion of petroleum resources and energy problems for future energy production [1–7]. Utilization of biomass as renewable, ubiquitous carbon sources to produce valuable biofuels and feedstock chemicals is one of the promising alternatives to the current petroleum-based chemical industrial technologies. Among various chemicals synthesized from cellulosic biomass, γ-valerolactone (GVL) is gaining considerable attention as a versatile building block, since it can be used as a fuel additive [8], solvent for biomass processing [9], as well as an ideal precursor for the production of hydrocarbons [10–14], polymers [10,15,16] and other valuable chemicals [10], thus has a great potential to reduce the consumption of petroleum-derived fossil fuels. In an ideal process currently proposed, GVL is produced from cellulosic biomass via hydrogenation of levulinic acid (LA) and its esters and the following acid-catalyzed intramolecular dehydration/dealcoholation step. LA and its esters are intermediate compounds produced by acid-catalyzed solvolysis of various cellulosic biomass such as cellulose, glucose, fructose, as well as 5-hydroxymethylfurfural (HMF) in water [17,18] and alcohols [19–27], respectively. The hydrogenation reaction of LA and its esters is generally conducted by using various heterogeneous precious metal particle catalysts such as Ru [28–32], Pd [33,34] and Pt [35], which can afford GVL in excellent yields under the presence of pressurized H_2, but high reaction temperatures and high H_2 pressures are still required to achieve high activities [36,37]. For the establishment of economical and ecological biomass conversion process, the reaction needs to be operated at low temperature/pressure conditions and the consumption of precious metals needs to be minimized [38].

Precious metal nanoparticles (NPs) are important catalysts in various chemical reactions, such as hydrogenation, dehydrogenation and oxidation, because of their unique structures and activities originating from their metal–metal bonds [39–41]. Their activities are known to be dependent on their particle size, structures, composition and the nature of support materials [42,43]. In order to maximize the catalytic activity of metal NPs and improve their reusability, they are conventionally immobilized on appropriate support materials with retaining their small particle size. Among numerous kinds of supports, mesoporous silica is frequently chosen

* Corresponding author at: Division of Materials and Manufacturing Science, Graduate School of Engineering, Osaka University, 2-1 Yamadaoka, Suita, Osaka 565-0871, Japan. Tel.: +81 6 6879 7457.
E-mail address: yamashita@mat.eng.osaka-u.ac.jp (H. Yamashita).

http://dx.doi.org/10.1016/j.cattod.2015.01.015
0920-5861/

as an ideal support owing to its pore diameter (2–20 nm) similar to the size of the metal NPs and the defined porous arrangement that can spatially-isolate the NPs. However, the metal NPs supported on the conventional mesoporous silicas usually suffer from leaching and particle aggregation during reactions and low-accessibility of reactant molecules because of the two-dimensionally-aligned long mesopore channel systems. One of the key issues for achieving high catalytic activity for the supported metal NPs is to develop a new method to highly-disperse and stabilize them by manipulating the morphology, porous structure and surface environment of mesoporous silicas. In regard to this issue, we have recently developed a method to disperse and stabilize guest species within the channels of mesoporous silica, in which the heteroatoms (especially Zr) imbedded within the matrix of mesoporous silica provide a productive effect to anchor and stabilize the guest species via intermolecular acid–base interactions [44,45]. Such effects are expected to be beneficial for dispersing and stabilizing metal NPs as well, and thus improve the catalytic performances of the metal NPs.

Herein, we demonstrate hydrogenation of levulinic acid and its esters into γ-valerolactone by using Ru NP catalysts confined in Zr-containing spherical mesoporous silica as a bifunctional catalyst. The Zr site imbedded within spherical mesoporous silica may have an ability to disperse and stabilize the Ru NPs, which may offer an improved stability and reusability of the Ru NP catalysts. Furthermore, the imbedded Zr sites may contribute to GVL selectivity owing to their acidic property to catalyze the dehydration/dealcoholation reaction steps [46–48]. To this end, a series of Zr-containing spherical mesoporous silica having P6mm hexagonal mesoporous structure with varied Zr content were synthesized by sol–gel process using cetyltrimethylammonium bromide (CTAB) as a pore-directing agent and tetraethylorthosilicate (TEOS) as a silicon source. The influences of Zr incorporation on porous structures, size of Ru NPs and catalytic performances (including activity, selectivity and stability) were investigated in detail. The activities of the catalysts were examined by the hydrogenation of levulinic acid (LA) and methyl levulinate (ML) at ambient reaction conditions and were compared with Ru NPs supported on the conventional silica materials.

2. Experimental

2.1. Synthesis of Zr-containing spherical mesoporous silica

The Zr-containing spherical mesoporous silicas (ZrSMS) with different Zr contents were synthesized according to the reported method with minor modifications [49,50]. Into an aqueous solution containing cetyltrimethylammonium bromide (CTAB, Wako Pure Chemical Ind., Ltd.) and aqueous ammonia (28%, Wako Pure Chemical Ind., Ltd.), tetraethylorthosilicate (TEOS, 95%, Wako Pure Chemical Ind., Ltd.) diluted in ethanol (1.0 M) was added rapidly at 50 °C under stirring. After stirring for 1 h, a mixture of TEOS and zirconium(IV) tetrapropoxide ($Zr(O^nPr)_4$, 70% in 1-propanol, Tokyo Chemical Ind. Co., Ltd.) in ethanol (0.2 M) was added dropwise under vigorous stirring and the mixture was continuously stirred for another 2 h at 50 °C. The molar ratio of the initial synthesis solution was adjusted to $Si:Zr:NH_3:CTAB:H_2O = 1.0:(0–0.1):28:0.25:2540$. The solution was then transferred to a teflon bottle, sealed and hydrothermally treated at 100 °C for 24 h under static conditions. Then, the resulting particles were collected by centrifugation at 18,000 rpm, washed several times with deionized water and ethanol, dried overnight and finally calcined at 550 °C for 6 h to remove the organic template. The samples were denoted as Zr*x*SMS, where *x* represents the Zr/Si molar ratio in the initial solution.

For comparison, a conventional mesoporous silica with large particle size (MCM-41) was prepared by a hydrothermal synthesis method using CTAB as an organic template and TEOS as a silicon source with the molar ratio of $Si:NH_3:CTAB:H_2O = 1.0:3.3:0.1:66$.

2.2. Synthesis of supported Ru NP catalysts

The supported Ru NP catalyst was synthesized by a conventional impregnation method and a following reduction treatment in a flow of H_2. 1.0 g of support was dispersed in 50 mL of aqueous solution containing 3.51 g of ruthenium(III) nitrosyl nitrate solution ($Ru(NO)(NO_3)_x(OH)_y$, 1.5% as Ru, Aldrich) and subjected to ultrasonication for 5 min. After stirring for 24 h at room temperature, the slurry was then placed in a rotary evaporator, and the water was removed under vacuum to facilitate the incorporation of the Ru(III) ions into the support. After drying at 100 °C, the sample was reduced in a flow of 10% H_2 in N_2 (100 mL/min) at 350 °C for 5 h with a ramping rate of 4 °C/min. The Ru loading was adjusted to 5 wt.%. The conventional mesoporous silica (MCM-41), fumed silica ($S_{BET} = 279\ m^2/g$, Wako Pure Chemical Ind., Ltd.) and zirconia ($S_{BET} = 112\ m^2/g$, Daiichi Kigenso Kagaku Kogyo Co., Ltd.) were also used as supports.

2.3. Characterization

X-ray diffraction (XRD) patterns were recorded on a Bruker AXS D8 Advance X-ray diffractometer with CuKα radiation (λ = 1.54056 Å, 40 kV to 40 mA). Nitrogen adsorption–desorption isotherms were measured at −196 °C by using Micromeritics ASAP2020. The samples were degassed at 300 °C under vacuum for 4 h prior to the measurements. The specific surface area was calculated by the BET (Brunauer–Emmett–Teller) method by using adsorption data ranging from $p/p_0 = 0.05–0.30$. The pore size distributions were obtained from the adsorption branches of the isotherms by the BJH (Barret–Joyner–Halenda) method. Transmission electron microscope (TEM) observations were performed with a FEI TITAN80-300 operated at 200 kV. Infrared spectra were recorded on a JASCO FTIR-6300 instrument in the spectral range 2000–400 cm^{-1} under vacuum with a resolution of 4 cm^{-1} using samples diluted with KBr. Dynamic light scattering (DLS) study was carried out on a Malvern Zetasizer Nano ZS at 25 °C in ethanol solution.

Temperature programmed desorption of NH_3 (NH_3-TPD) was performed by using a BELCAT-B system (BEL Japan, Inc.) equipped with an on-line thermal conductivity detector. The samples were pretreated under a He flow (50 mL/min) at 600 °C for 1 h, allowed to cool to 50 °C and subsequently exposed to flowing 5% NH_3/He gas (50 mL/min) for 1 h. After purging at 50 °C for 30 min with He, NH_3-TPD was carried out between 50 and 600 °C under a He flow (30 mL/min) with a ramping rate of 10 °C/min.

2.4. Procedures for catalytic reactions

Hydrogenation of LA and ML was performed in a 60 mL cylindrical stainless steel autoclave reactor (EYELA, Inc.) equipped with a bourdon pressure gauge. In a typical reaction, catalyst (Ru 0.5 mol%), substrate (5 mmol) and solvent (water or methanol, 10 mL) were introduced into the reactor, which was then sealed, purged and pressurized with 0.5 MPa of H_2 and then heated at 70 °C with magnetic stirring. After the allotted reaction time, a portion of the reaction mixture was withdrawn by filtration and then analyzed by a gas chromatograph (Shimadzu GC-14B) with a flame ionization detector equipped with a capillary column (ULBON HR-20M; 0.53 mm × 30 m; Shinwa Chemical Ind., Ltd.). Conversion of substrate and yields of products were quantified by using bis(2-methoxyethyl)ether as an internal standard. To study the catalyst

Please cite this article in press as: Y. Kuwahara, et al., Ru nanoparticles confined in Zr-containing spherical mesoporous silica containers for hydrogenation of levulinic acid and its esters into γ-valerolactone at ambient conditions, Catal. Today (2015), http://dx.doi.org/10.1016/j.cattod.2015.01.015

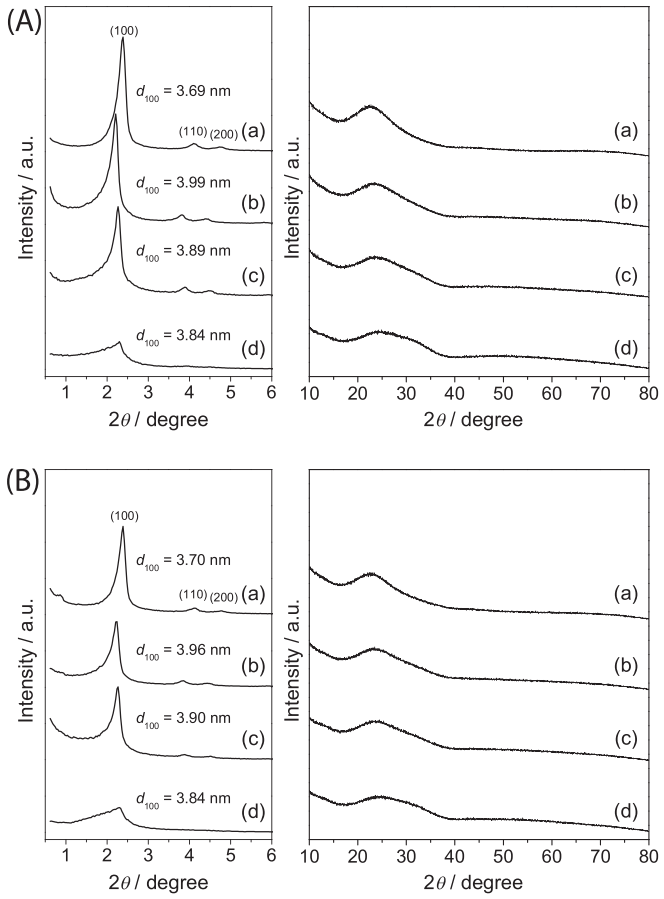

Fig. 1. XRD patterns of (a) SMS, (b) Zr2.5SMS, (c) Zr5SMS and (d) Zr10SMS (A) before and (B) after the deposition of 5 wt.% Ru. Several diffraction planes associated with 2D hexagonal mesoporous structure (P6mm) are indicated for SMS.

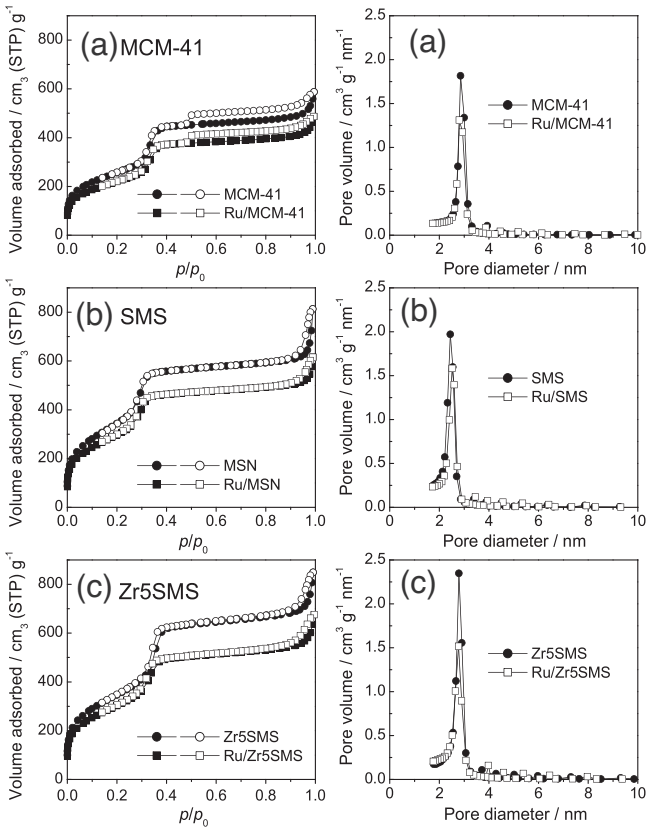

Fig. 2. (Left) Nitrogen adsorption–desorption isotherms and (right) BJH pore size distributions of MCM-41, SMS and Zr5SMS materials before and after the deposition of 5 wt.% Ru. Filled and empty symbols in the left represent adsorption and desorption branches, respectively. The pore size distribution curves were calculated by BJH method from the adsorption branches.

reusability, the spent catalyst was recovered by centrifugation, washed with water and acetone, dried under vacuum, and then subjected to the next catalytic run.

3. Results and discussion

3.1. Structural analysis

The structural characteristics of a series of ZrSMS materials were investigated by XRD measurement, N_2 physisorption and TEM. Fig. 1A and B shows XRD patterns of ZrSMS materials with varied Zr contents (0–10 mol% per Si) before and after the deposition of 5 wt.% Ru NPs, respectively. The as-synthesized ZrSMS all exhibited several distinct peaks in low angle region, which are indexed as the (1 0 0), (1 1 0) and (2 0 0) reflections of the 2D hexagonal mesoporous structure with P6mm symmetry (Fig. 1A). When 10 mol% of Zr per Si was added, an appreciable decrease in XRD intensity was observed (Fig. 1A(d)), indicating that introduction of an excess amount of Zr (>10 mol%) leads to a disordering of the pore arrangement. In high angle XRD patterns, the ZrSMS materials exhibited no diffraction peaks except for the broad peak attributable to amorphous silicate phase (2θ = 15–40°), suggesting that the Zr atoms are uniformly incorporated within the silica matrix by isomorphous substitution at all Zr levels. After the deposition of 5 wt.% of Ru NPs, no significant change was observed in the XRD patterns (cf. Fig. 1A and B). The *d*-spacing values calculated from the position of (1 0 0) reflection remained almost unchanged, and the crystalline phase for Ru metals were undetectable in all cases. These results imply that the Ru NPs are present as ultrasmall nanoparticles.

N_2 adsorption–desorption isotherms of MCM-41, SMS and Zr5SMS before and after the deposition of 5 wt.% of Ru NPs are shown in Fig. 2. All the samples showed typical type IV isotherms with clear inflections at around p/p_0 = 0.3 and with narrow pore distributions centered at around 2.4–2.8 nm, showing the similar mesopore characteristics between the ZrSMS materials and the conventional MCM-41. The textural parameters of the as-synthesized ZrSMS materials obtained from the N_2 isotherms are summarized in Table 1. It should be noted that the specific surface areas and total pore volumes of ZrSMS materials (S_{BET} = 1000–1300 m^2/g, V_{total} = 1.1–1.3 cm^3/g) were quite larger than those of MCM-41 (S_{BET} = 923 m^2/g, V_{total} = 0.86 cm^3/g). This is probably due to the existence of interparticle voids caused by silica particle aggregation, which has been reflected in the N_2 isotherms as steep increases at high relative pressure region (p/p_0 > 0.90). It is presumable that such an enlarged surface area and pore volume are especially effective for mass transportation of guest reactants within the mesopore channels during the catalytic reactions. Addition of a small amount of Zr (<10 mol% per Si) during the synthesis of SMS scarcely affected the structural parameters; however, 10 mol% Zr addition caused a slight decrease of both surface area and pore volume, being coincided with the XRD result (Table 1). At higher percentage of Zr (>10 mol% per Si), the ordered structure of SMS appears to degrade and accordingly results in a reduced mesoporosity, yet it can still be regarded as a periodic mesoporous material. Ru NPs-loaded samples also displayed as similar type IV isotherms with clear reflections as those before Ru NPs deposition, demonstrating the retention of defined mesopore channels. The adsorbed nitrogen quantities slightly decreased after the deposition of Ru NPs; however, they still retained most

Please cite this article in press as: Y. Kuwahara, et al., Ru nanoparticles confined in Zr-containing spherical mesoporous silica containers for hydrogenation of levulinic acid and its esters into γ-valerolactone at ambient conditions, Catal. Today (2015), http://dx.doi.org/10.1016/j.cattod.2015.01.015

Table 1
Textural properties of support materials used in this study.

Sample	EDX		DLS	N_2 physisorption			NH_3-TPD	
	Zr/Si (initial gel)	Zr/Si[a] (final solid)	Average particle diameter (nm)	S_{BET}[b] (m^2/g)	V_{total}[c] (cm^3/g)	D_p[d] (nm)	Acid site[e] (mmol/g)	Acid density[f] ($\mu mol/m^2$)
SMS	0	0	180	1297	1.25	2.4	0.069	0.05
Zr2.5SMS	0.025	0.05	226	1275	1.28	2.8	0.23	0.18
Zr5SMS	0.05	0.08	248	1267	1.31	2.8	0.29	0.23
Zr10SMS	0.10	0.17	256	1015	1.10	2.8	0.35	0.34
MCM-41	–	–	–	923	0.86	2.8	0.071	0.08
SiO_2	–	–	–	279	0.60	N.D.	0.033	0.12
ZrO_2	–	–	–	112	0.29	8.6	–	–

[a] Molar ratio determined by EDX analysis.
[b] Specific surface area calculated by BET method from N_2 adsorption data ranging from $p/p_0 = 0.05$ to 0.30.
[c] Total pore volume determined by nitrogen adsorption at a relative pressure of 0.99.
[d] Average pore diameter determined by BJH method.
[e] Amount of NH_3 chemisorbed per gram of sample.
[f] Calculated by the equation: [Acid density ($\mu mol/m^2$)] = [Acid amount (mmol/g)]/[specific surface area of sample (m^2/g)] × 1000.

Table 2
Textural properties of Ru/ZrSMS and supported Ru catalysts.

Sample	EDX	TEM	N_2 physisorption		
	Ru (wt.%)	Particle diameter of Ru[a] (nm)	S_{BET}[b] (m^2/g)	V_{total}[c] (cm^3/g)	D_p[d] (nm)
Ru/SMS	4.57	1.49	1107	0.95	2.5
Ru/Zr2.5SMS	4.47	1.28	1083	1.08	2.8
Ru/Zr5SMS	4.52	1.24	1106	1.05	2.8
Ru/Zr10SMS	4.49	1.32	1006	1.04	2.8
Ru/MCM-41	4.50	1.72	795	0.75	2.8
Ru/SiO_2	–	–	215	1.24	N.D.
Ru/ZrO_2	–	–	76	0.26	16.5

[a] Average particle diameter calculated from 100 particles randomly selected from the TEM images.
[b] Specific surface area calculated by BET method from N_2 adsorption data ranging from $p/p_0 = 0.05$ to 0.30.
[c] Total pore volume determined by nitrogen adsorption at a relative pressure of 0.99.
[d] Average pore diameter determined by BJH method.

of their surface areas (S_{BET} = 1000–1100 m^2/g) and pore volumes (V_{total} = 1.0–1.1 cm^3/g), which are larger than those of Ru/MCM-41 (S_{BET} = 795 m^2/g, V_{total} = 0.75 cm^3/g) and Ru/SiO_2 (S_{BET} = 215 m^2/g, V_{total} = 1.24 cm^3/g) (Table 2).

Fig. 3 shows high resolution transmission electron microscope (HRTEM) images, high-angle annular dark field scanning TEM (HAADF-STEM) images and the corresponding Ru particle size distribution diagrams of Ru/MCM-41, Ru/SMS and Ru/Zr5SMS. The HRTEM image of the conventional Ru/MCM-41 showed long mesopore channels linearly aligned at regular intervals (Fig. 3a). The average pore size was estimated to be ca. 2.85 nm, agreeing well with the one determined based on the N_2 adsorption measurement. HAADF-STEM image of Ru/MCM-41 clearly visualized nano-sized Ru particles randomly distributed in the particles, with a relatively broad size distribution ranged from 1.0 to 3.0 nm and with an average size of 1.72 nm. On the other hand, the HRTEM image of Ru/SMS displayed monodispersed spherical particles having three-dimensionally-oriented short mesopore channels throughout the particles (Fig. 3b). The HRTEM image of Ru/Zr5SMS showed rectangle silica particles, and its particle size was apparently larger than that of Ru/SMS (Fig. 3c). From the DLS study, the primary silica particle size of Ru/SMS and Ru/Zr5SMS was determined to be 180 and 248 nm, respectively (see Table 1; Ru/Zr2.5SMS and Ru/Zr10SMS also showed similar particle morphologies and silica particle sizes). This difference in particle size of silica is likely due to the different grain growth rate during the synthesis caused by the addition of zirconium alkoxide. HAADF-STEM images of Ru/SMS and Ru/Zr5SMS showed Ru NPs uniformly dispersed along with the short mesopore channels without any agglomeration. The size of Ru NPs was distributed in the range of 0.8–2.0 nm and the average particle size was determined to be 1.49 and 1.24 nm for Ru/SMS and Ru/Zr5SMS, respectively, which were obviously smaller than those in Ru/MCM-41. The formation of such ultrasmall Ru NPs is possibly due to the smaller silica particle size and the short mesopore channels of SMS which facilitate incorporation of Ru species inside the pore channels [51] as well as the anchoring effect of amphoteric Zr sites which stabilize and prevent the Ru NPs from growing into big particles [44,45].

3.2. Investigation of chemical environment of Zr atoms

The Zr/Si atomic ratio in the final solids were higher than the ones in the initial synthesis solutions (see Table 1), suggesting that some fraction of TEOS were not incorporated into the final solids under the applied synthesis conditions, presumably due to the formation of unrecoverable, soluble silica nano-clusters. To investigate the chemical environment of Zr atoms, FT-IR spectra were taken for the series of ZrSMS materials (Fig. 4). Siliceous SMS showed several characteristic infrared absorption bands at around 460, 805, 1085 cm^{-1} which are assignable to the bending, symmetric stretching and asymmetric stretching vibration of the Si–O–Si bond, respectively [26,47]. The band at 1630 cm^{-1} is the band associated with O–H bending vibration of adsorbed H_2O molecules and surface silanol groups [26,47]. Zr-containing SMS solids showed increased intensity of the band located at around 961 cm^{-1} which is a diagnostic band of the Si–O–Zr bond [26,47]. As increasing the Zr content in the samples, the relative intensity of this band (I_{961}/I_{1085}) increased in the order of SMS (0.33) < Zr2.5SMS (0.50) < Zr5SMS (0.53) < Zr10SMS (0.58), indicating an incorporation of increased amount of Zr within SMS solid. In addition, specific bands assignable to Zr–O–Zr bond (normally observed in the range of 500–800 cm^{-1}) were not observed [27]. These results indicate the incorporated Zr atoms are dominantly present as isolated Zr atoms within the silica matrix of SMS.

Please cite this article in press as: Y. Kuwahara, et al., Ru nanoparticles confined in Zr-containing spherical mesoporous silica containers for hydrogenation of levulinic acid and its esters into γ-valerolactone at ambient conditions, Catal. Today (2015), http://dx.doi.org/10.1016/j.cattod.2015.01.015

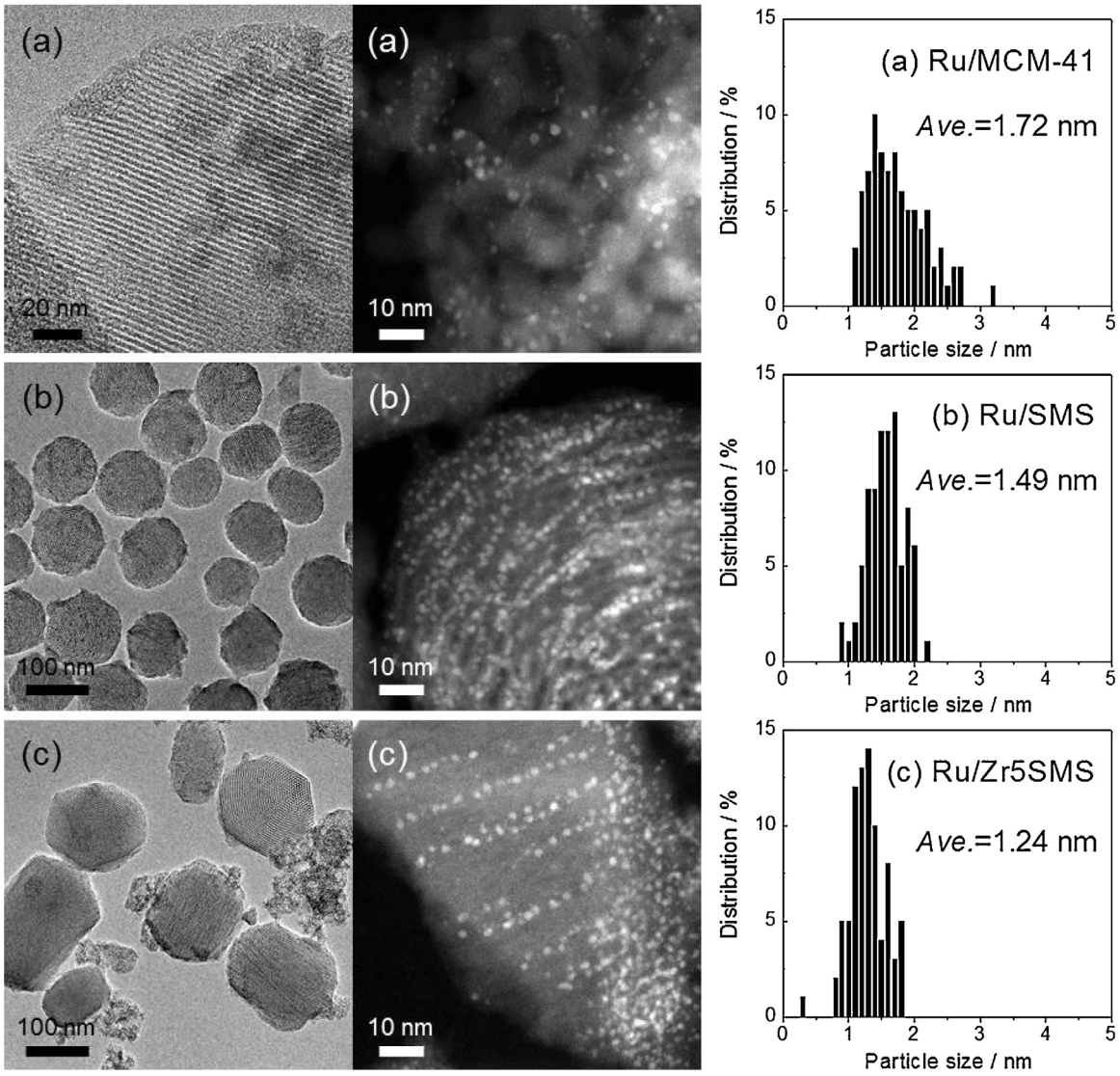

Fig. 3. (Left) HRTEM images, (middle) HAADF-STEM images and (right) Ru particle size distribution diagrams of (a) Ru/MCM-41, (b) Ru/SMS and (c) Ru/Zr5SMS.

3.3. Hydrogenation of levulinic acid and its esters

Levulinic acid is generally produced by acid-catalyzed hydrolysis of sugars, which results in a mixture of levulinic acid and formic acid in water [17,18]. In a similar manner, in an ideal biomass conversion process, levulinate esters are obtained from cellulosic biomass sources in the form of mixtures with the corresponding alcohols [19–27]. In addition, for the establishment of greener and cost-effective biomass conversion process, the reaction needs to be operated at lower temperature/pressure conditions and using smaller amount of catalyst. On this account, in this study, we performed the hydrogenation of levulinic acid and methyl levulinate at 70 °C under 0.5 MPa of H_2 with low catalyst loading (0.5 mol% Ru) using water and methanol as reaction media, respectively.

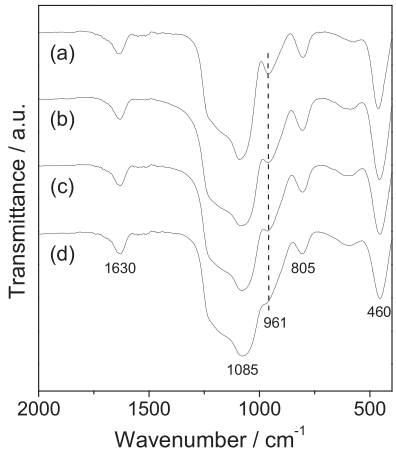

Fig. 4. FTIR spectra of (a) SMS, (b) Zr2.5SMS, (c) Zr5SMS and (d) Zr10SMS.

The reaction profiles in the hydrogenation of LA over the supported Ru catalysts are shown in Fig. 5, and the conversions of LA and yields of GVL after 4 h of the reaction are also listed in Table 3. The prepared Ru/ZrSMS catalysts showed similar reaction rates in both LA conversion (Fig. 5A) and GVL production (Fig. 5B), affording ~99% LA conversions and ~95% GVL yields after 4 h of reaction, and the intermediate hydrogenated product, 4-hydroxy pentanoic acid (4-HPA), was scarcely produced in all cases. This high selectivity to GVL is because of the strong acidity of LA (pK_a = 4.59) which can self-catalyze the dehydration of 4-HPA to form GVL, thereby making the effect of Zr acidity less significant. Ru/MCM-41 and Ru/SiO_2 as reference catalysts displayed subpar catalytic activities (88–89% LA conversions and 84–85% GVL yields), whereas Ru

Please cite this article in press as: Y. Kuwahara, et al., Ru nanoparticles confined in Zr-containing spherical mesoporous silica containers for hydrogenation of levulinic acid and its esters into γ-valerolactone at ambient conditions, Catal. Today (2015), http://dx.doi.org/10.1016/j.cattod.2015.01.015

Table 3
Hydrogenation of LA and ML into GVL over supported Ru catalysts

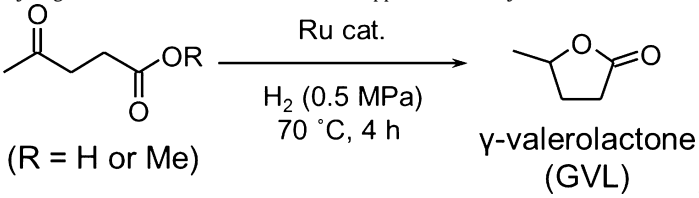

Catalyst	LA hydrogenation[a]		ML hydrogenation[b]	
	Conv. (%)	GVL yield (%)	Conv. (%)	GVL yield (%)
Ru/SMS	99.2	95.6	80.1	31.9
Ru/Zr2.5SMS	97.0	93.4	99.7	40.0
Ru/Zr5SMS	96.2	92.1	99.8	67.1
Ru/Zr10SMS	98.4	94.5	99.8	46.9
Ru/MCM-41	89.0	84.1	77.8	27.8
Ru/SiO_2	88.3	84.8	66.5	33.9
Ru/ZrO_2	69.0	66.9	64.7	25.8

[a] *Reaction conditions:* catalyst (Ru 0.5 mol%), LA (5 mmol), water (10 mL), H_2 (0.5 MPa), 70 °C, 4 h.
[b] *Reaction conditions:* catalyst (Ru 0.5 mol%), ML (5 mmol), MeOH (10 mL), H_2 (0.5 MPa), 70 °C, 4 h.

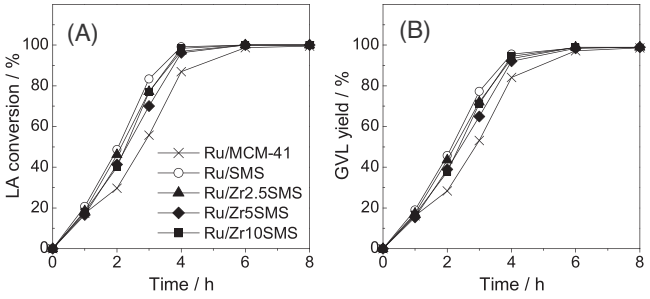

Fig. 5. Reaction profiles in hydrogenation of levulinic acid (LA) over supported Ru catalysts: (A) conversion of LA, (B) yield of GVL. *Reaction conditions:* catalyst (Ru 0.5 mol%), LA (5 mmol), water (10 mL), H_2 (0.5 MPa), 70 °C.

particles supported on ZrO_2 provided a markedly decreased activity (69.0% LA conversion and 66.9% GVL production) under the same reaction conditions, suggesting a bigger particle size of Ru on these supports. It is assumable that, in this reaction, the hydrogenation on Ru nanoparticles is the rate-determining step and that spherical mesoporous silicas combining both large surface areas and short mesopore channels are promising supports for creating small and active Ru NP catalysts.

Considerably different reaction kinetics was observed in the hydrogenation of ML into GVL (Fig. 6). This reaction also proceeds through a tandem pathway involving hydrogenation of ML to 4-hydroxy pentanoic acid methyl ester (4-HPME), followed by dealcoholation of 4-HPME to GVL, in the latter step acid site plays a key role for efficient transformation into GVL [31,32].

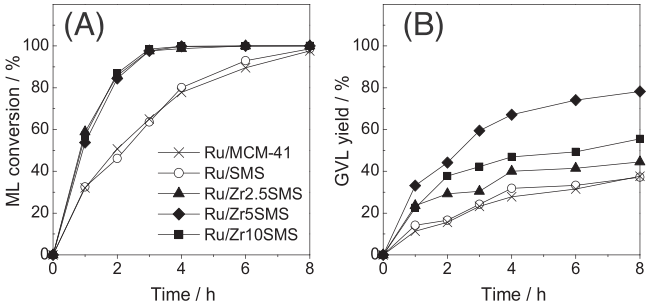

Fig. 6. Reaction profiles in hydrogenation of methyl levulinate (ML) over supported Ru catalysts: (A) conversion of ML, (B) yield of GVL. *Reaction conditions:* catalyst (Ru 0.5 mol%), ML (5 mmol), methanol (10 mL), H_2 (0.5 MPa), 70 °C.

During the reaction, no other byproducts were formed except for 4-HPME and GVL. The Ru NP catalysts supported on the series of ZrSMS materials (Ru NP size: 1.24–1.32 nm) afforded >99% ML conversions after 4 h of reaction (Fig. 6A and Table 3), whereas Ru NPs supported on unmodified normal SMS (Ru NP size: 1.49 nm) and bulky MCM-41 (Ru NP size: 1.72 nm) gave moderate ML conversions (77.8–80.1%), demonstrating the impact of Ru NP size on the hydrogenation step of ML. More significantly, the rate of GVL production increased in the order of: Ru/MCM-41 ≈ Ru/SMS < Ru/Zr2.5SMS < Ru/Zr10SMS < Ru/Zr5SMS (Fig. 6B), suggesting that Zr sites play a crucial role in the latter dealcoholation step. NH_3-TPD of ZrSMS supports clearly revealed that the Zr sites imbedded within silica matrix act as acidic sites on the support surface, and the density of acidic sites monotonically increases as the Zr content in the samples increases (0.18–0.34 μmol/m^2), while pure siliceous SMS and MCM-41 have almost no acidity on their surfaces (0.05–0.08 μmol/m^2) (see Table 1). Therefore, we can attribute the increase in the GVL production rate to the combined effect of (i) ultrasmall size of Ru NPs that can effectively catalyze hydrogenation of ML to 4-HPME and (ii) improved acidity of support material that can promote the intramolecular dealcoholation of 4-HPME to GVL. Among the catalysts examined in this study, Ru/Zr5SMS accommodating the smallest Ru NPs and with modest Zr content was found to be the most effective catalyst, affording 67.1% GVL yield from ML at 70 °C under 0.5 MPa of H_2 after 4 h of reaction. Ru/Zr10SMS having the highest acid density exhibited a lower GVL production rate rather than Ru/Zr5SMS catalyst. This is probably due to the subpar pore characteristics of Zr10SMS support (see Table 1), hindering the access of intermediate products (4-HPME) to the Zr acid sites. It is also worth noting that the synthesized catalyst was also active for the hydrogenation of other levulinate esters, such as ethyl levulinate (EL) and butyl levulinate (BL), while the selectivity to GVL was considerably lower than the case for ML hydrogenation (see Fig. A in the supporting information).

3.4. Effect of acid additives

To further improve the GVL yield in the hydrogenation reaction of ML, addition of acids was examined using Ru/Zr5SMS as a catalyst. Table 4 shows conversions of ML and yields of GVL as well as the estimated acidity of the acid additives. Ru/Zr5SMS as a baseline sample provided 99.8% ML conversion and 67.1% GVL yield after 4 h of reaction (Entry 1). The reaction was significantly accelerated in the presence of the solid acid co-catalysts; when 1.0–3.0 wt.% of

Please cite this article in press as: Y. Kuwahara, et al., Ru nanoparticles confined in Zr-containing spherical mesoporous silica containers for hydrogenation of levulinic acid and its esters into γ-valerolactone at ambient conditions, Catal. Today (2015), http://dx.doi.org/10.1016/j.cattod.2015.01.015

Table 4
Effect of acid additives in the hydrogenation of ML in MeOH with Ru/Zr5SMS[a]

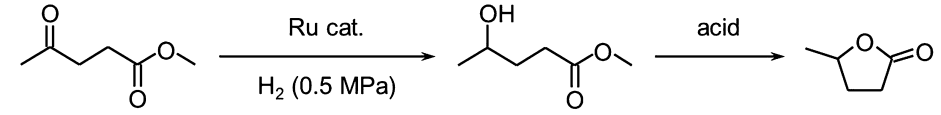

Methyl levulinate (ML) | 4-hydroxy pentanoic acid methyl ester | γ-valerolactone (GVL)

Entry	Acid[b]	Loading (wt.%)	Acidity (H^+ mmol/g)	Conv. (%)	GVL yield (%)
1	None	–	–	99.8	67.1
2	Amberlyst-15	1.0	4.7	>99.9	85.3
3		3.0	4.7	>99.9	92.1
4	H-Y(30)	1.0	0.62	>99.9	89.0
5		3.0	0.62	>99.9	96.1
6	H-beta(25)	1.0	1.0	>99.9	77.8
7	H-ZSM-5(30)	1.0	1.2	>99.9	75.5
8	$H_3PW_{12}O_{40}$	1.0	N.D.	48.3	31.9
9	*p*-TSA	1.0	5.8	11.5	5.7

[a] *Reaction conditions:* catalyst (Ru/Zr5SMS, Ru 0.5 mol%), ML (5 mmol), MeOH (10 mL), H_2 (0.5 MPa), 70 °C, 4 h.
[b] The values in the parentheses represent SiO_2/Al_2O_3 ratios of zeolites.

Amberlyst-15, a commercially available acidic resin, was added into the reaction medium, faster reaction rates and improved GVL selectivities were attained, giving >99.9% ML conversion and 85.3–92.1% GVL yield after 4 h, because of the ability of the acid to promote the dealcoholation of 4-HPME to yield GVL (Entries 2 and 3; for detailed reaction kinetics, see Fig. B in the supporting information). Addition of H^+-type zeolites (H-Y(30), H-beta(25) and H-ZSM-5(30)) was also effective for improving the reaction rates (Entries 4–7), among which H-Y(30) having modest acidity worked as the best acid co-catalyst, yielding 89.0–96.1% GVL after 4 h of reaction (Entries 4 and 5). On the contrary, addition of homogeneous acids, such as soluble heteropolyacid ($H_3PW_{12}O_{40}$) and *p*-toluenesulfonic acid (*p*-TSA), resulted in lower reaction rates (Entries 8 and 9). Judging from the reaction kinetics data, these homogeneous acids are likely to have an easy access to the Ru NPs and readily deactivate them. These results clearly demonstrate the importance of site-isolation between Ru NPs and acid sites [32,52].

3.5. Reusability of catalyst

To examine the reusability of the catalyst, several selected catalysts were subjected to multiple catalytic cycles in the hydrogenation of LA. Fig. 7 compares catalytic activities of Ru/MCM-41, Ru/SMS and Ru/Zr5SMS over five repeated cycles under the standard conditions (i.e., 0.5 mol% Ru catalyst, 70 °C, 0.5 MPa H_2, 4 h). Ru NPs supported on the conventional MCM-41 showed a continual activity reduction during moderate cycling and eventually lost almost half of its initial activity after five catalytic cycles. This considerable activity reduction can be associated with Ru NPs agglomeration into bigger particles during its repeated use, otherwise, the substantial loss of Ru NPs caused by elution into reaction medium (for XRD patterns and HAADF-STEM images after the reaction, see Fig. C in the supporting information). In contrast, Ru NPs supported on SMS and Zr5SMS catalysts retained more than 90% of their initial activities after the same number of cycles, demonstrating their superior reusability. This markedly increased catalyst reusability is likely due to the high dispersibility of Ru NPs confined inside the mesopore channels of the SMS materials (as shown in HAADF-STEM images) and possibly due to the anchoring effect of the Zr sites which stabilize and prevent the Ru NPs from growing into bigger particles. XRD analysis and TEM observation of the catalysts after the repeated catalytic cycles indicated that the Ru NPs on the SMS materials still retained their inherent particle sizes, while Ru/MCM-41 showed a more increased fraction of agglomerated Ru NPs with the size of >2 nm which was detectable in XRD patterns (Fig. C), supporting the above hypothesis.

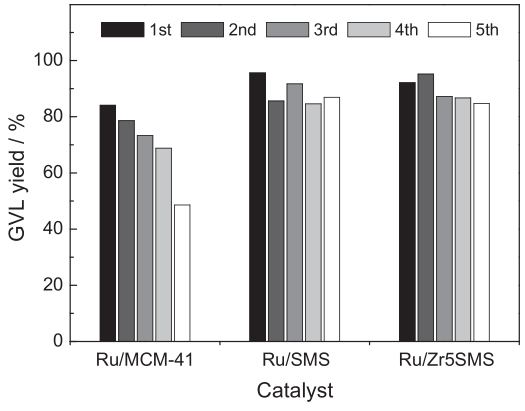

Fig. 7. Catalytic activity of Ru/MCM-41, Ru/SMS and Ru/Zr5SMS over 5 repeated cycles in the hydrogenation of LA. *Reaction conditions:* catalyst (Ru 0.5 mol%), LA (5 mmol), water (10 mL), H_2 (0.5 MPa), 70 °C, 4 h.

4. Conclusions

Ru NPs confined in spherical mesoporous silica nanocontainers (SMS) were demonstrated to be more effective catalyst in the hydrogenation of levulinic acid and its esters at ambient reaction conditions (70 °C, 0.5 MPa H_2) compared to those supported on the conventional silica materials. TEM observation revealed that the ultrasmall Ru NPs with the particle size of less than 2 nm were highly dispersed inside the periodically ordered short mesopore channels without any agglomeration. Further functionalization of SMS by Zr afforded a bifunctional catalyst, Ru/ZrSMS, which showed superior catalytic activities especially in the hydrogenation of levulinate esters owing to the ultrasmall size of Ru NPs and the ability of Zr acid sites to promote the intramolecular dealcoholation of 4-hydroxy pentanoic acid methyl ester to produce GVL. Among the catalysts examined, Ru NPs supported on 5 mol% Zr-doped SMS was found to be the best catalyst in terms of catalytic activity, selectivity and reusability, making it promising heterogeneous catalyst for GVL production from biomass-derived levulinic acid and its esters at ambient conditions. We expect that the functionality can further be tunable by altering the kind of metal NPs and the heteroatom species imbedded in the silica matrix, which would bring us a method to synthesize new type of bifunctional catalysts

Please cite this article in press as: Y. Kuwahara, et al., Ru nanoparticles confined in Zr-containing spherical mesoporous silica containers for hydrogenation of levulinic acid and its esters into γ-valerolactone at ambient conditions, Catal. Today (2015), http://dx.doi.org/10.1016/j.cattod.2015.01.015

especially efficient for the chemical reactions that proceed through tandem reaction pathways.

Acknowledgements

This work was financially supported by the Grant-in-Aid from Frontier Research Base for Global Young Researchers, Osaka University, and the Grant-in-Aid for Scientific Research (KAKENHI) from the Ministry of Education, Culture, Sports, Science and Technology (No. 26220911). A part of this work was also performed under a management of 'Elements Strategy Initiative for Catalysts & Batteries (ESICB)' supported by MEXT.

Appendix A. Supplementary data

Supplementary data associated with this article can be found, in the online version, at http://dx.doi.org/10.1016/j.cattod.2015.01.015.

References

[1] A. Corma, S. Iborra, A. Velty, Chem. Rev. 107 (2007) 2411–2502.
[2] J.N. Chheda, G.W. Huber, J.A. Dumesic, Angew. Chem. Int. Ed. 46 (2007) 7164–7183.
[3] D.M. Alonso, J.Q. Bond, J.A. Dumesic, Green Chem. 12 (2010) 1493–1513.
[4] J.J. Bozell, G.R. Petersen, Green Chem. 12 (2010) 539–554.
[5] J.C. Serrano-Ruiz, R. Luque, A. Sepúlveda-Escribano, Chem. Soc. Rev. 40 (2011) 5266–5281.
[6] J.C. Serrano-Ruiz, A. Pineda, A.M. Balu, R. Luque, J.M. Campelo, A.A. Romero, J.M. Ramos-Fernández, Catal. Today 195 (2012) 162–168.
[7] M.J. Climent, A. Corma, S. Iborra, Green Chem. 16 (2014) 516–547.
[8] I.T. Horváth, H. Mehdi, V. Fábos, L. Boda, L.T. Mika, Green Chem. 10 (2008) 238–242.
[9] J.M.R. Gallo, D.M. Alonso, M.A. Mellmer, J.A. Dumesic, Green Chem. 15 (2013) 85–90.
[10] D.M. Alonso, S.G. Wettstein, J.A. Dumesic, Green Chem. 15 (2013) 584–595.
[11] J.Q. Bond, D.M. Alonso, D. Wang, R.M. West, J.A. Dumesic, Science 327 (2010) 1110–1114.
[12] J.Q. Bond, D.M. Alonso, R.M. West, J.A. Dumesic, Langmuir 26 (2010) 16291–16298.
[13] J.C. Serrano-Ruiz, D. Wang, J.A. Dumesic, Green Chem. 12 (2010) 574–577.
[14] D.J. Braden, C.A. Henao, J. Heltzel, C.C. Maravelias, J.A. Dumesic, Green Chem. 13 (2011) 1755–1765.
[15] L.E. Manzer, Appl. Catal. A 272 (2004) 249–256.
[16] J.-P. Lange, J.Z. Vestering, R.J. Haan, Chem. Commun. (2007) 3488–3490.
[17] P.P.T. Sah, S.-Y. Ma, J. Am. Chem. Soc. 52 (1930) 4880–4883.
[18] W. Zeng, D. Cheng, H. Zhang, F. Chen, X. Zhan, Reac. Kinet. Mech. Cat. 100 (2010) 377–384.
[19] J.-P. Lange, W.D. van de Graaf, R.J. Haan, ChemSusChem 2 (2009) 437–441.
[20] L. Peng, L. Lin, J. Zhang, J. Shi, S. Liu, Appl. Catal. A 397 (2011) 259–265.
[21] K. Tominaga, A. Mori, Y. Fukushima, S. Shimada, K. Sato, Green Chem. 13 (2011) 810–812.
[22] X. Hu, C.-Z. Li, Green Chem. 13 (2011) 1676–1679.
[23] X. Hu, Y. Song, L. Wu, M. Gholizadeh, C.-Z. Li, ACS Sustainable Chem. Eng. 1 (2013) 1593–1599.
[24] A. Démolis, N. Essayem, F. Rataboul, ACS Sustainable Chem. Eng. 2 (2014) 1338–1352.
[25] P. Demma Carà, R. Ciriminna, N.R. Shiju, G. Rothenberg, M. Pagliaro, ChemSusChem 7 (2014) 835–840.
[26] Y. Kuwahara, T. Fujitani, H. Yamashita, Catal. Today 237 (2014) 18–28.
[27] Y. Kuwahara, W. Kaburagi, K. Nemoto, T. Fujitani, Appl. Catal. A 476 (2014) 186–196.
[28] Z.-p. Yan, L. Lin, S. Liu, Energy Fuels 23 (2009) 3853–3858.
[29] M.G. Al-Shaal, W.R.H. Wright, R. Palkovits, Green Chem. 14 (2012) 1260–1263.
[30] A.M.R. Galletti, C. Antonetti, V. De Luise, M. Martinelli, Green Chem. 14 (2012) 688–694.
[31] J.M. Nadgeri, N. Hiyoshi, A. Yamaguchi, O. Sato, M. Shirai, J. Jpn. Petrol. Inst. 55 (2012) 376–379.
[32] J.M. Nadgeri, N. Hiyoshi, A. Yamaguchi, O. Sato, M. Shirai, Appl. Catal. A 470 (2014) 215–220.
[33] K. Yan, C. Jarvis, T. Lafleur, Y. Qiao, X. Xie, RSC Adv. 3 (2013) 25865–25871.
[34] K. Yan, T. Lafleur, G. Wu, J. Liao, C. Ceng, X. Xie, Appl. Catal. A 468 (2013) 52–58.
[35] B. Chen, F. Li, Z. Huang, T. Lu, Y. Yuan, G. Yuan, ChemSusChem 7 (2014) 202–209.
[36] M.J. Climent, A. Corma, S. Iborra, Green Chem. 13 (2011) 520–540.
[37] W.R.H. Wright, R. Palkovits, ChemSusChem 5 (2012) 1657–1667.
[38] Y. Kuwahara, W. Kaburagi, T. Fujitani, RSC Adv. 4 (2014) 45848–45855.
[39] J.P. Wilcoxon, B.L. Abrams, Chem. Soc. Rev. 35 (2006) 1162–1194.
[40] S.-G. Kwon, T.-G. Hyeon, Acc. Chem. Res. 41 (2008) 1696–1709.
[41] K. Mori, N. Yoshioka, Y. Kondo, T. Takeuchi, H. Yamashita, Green Chem. 11 (2009) 1337–1342.
[42] K. Mori, A. Kumami, M. Tomonari, H. Yamashita, J. Phys. Chem. C 113 (2009) 16850–16854.
[43] K. Mori, H. Yamashita, J. Jpn. Petrol. Inst. 54 (2011) 1–14.
[44] Y. Kuwahara, D.-Y. Kang, J.R. Copeland, P. Bollini, C. Sievers, T. Kamegawa, H. Yamashita, C.W. Jones, Chem. Eur. J. 18 (2012) 16649–16664.
[45] Y. Kuwahara, D.-Y. Kang, J.R. Copeland, N.A. Brunelli, S.A. Didas, P. Bollini, C. Sievers, T. Kamegawa, H. Yamashita, C.W. Jones, J. Am. Chem. Soc. 134 (2012) 10757–10760.
[46] S.-Y. Chen, J.-F. Lee, S. Cheng, J. Catal. 270 (2010) 196–205.
[47] D.M. Do, S. Jaenicke, G.-K. Chuah, Catal. Sci. Technol. 2 (2012) 1417–1424.
[48] J. Iglesias, M.D. Gracia, R. Luque, A.A. Romero, J.A. Melero, ChemCatChem 4 (2012) 379–386.
[49] Q. Cai, Z.-S. Luo, W.-Q. Pang, Y.-W. Fan, X.-H. Chen, F.-Z. Cui, Chem. Mater. 13 (2001) 258–263.
[50] J. Chen, F. Lu, J. Zhang, W. Yu, F. Wang, J. Gao, J. Xu, ChemCatChem 5 (2013) 2822–2826.
[51] S. Okada, T. Urata, T. Kamegawa, K. Mori, H. Yamashita, Chem. Lett. 40 (2011) 609–611.
[52] Z. Wu, S. Ge, C. Ren, M. Zhang, A. Yip, C. Xu, Green Chem. 14 (2012) 3336–3343.

Please cite this article in press as: Y. Kuwahara, et al., Ru nanoparticles confined in Zr-containing spherical mesoporous silica containers for hydrogenation of levulinic acid and its esters into γ-valerolactone at ambient conditions, Catal. Today (2015), http://dx.doi.org/10.1016/j.cattod.2015.01.015